ADVANCED MATERIALS

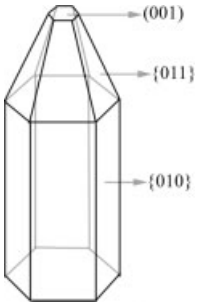

Fig. 7. Scheme illustrating the growth pattern of a β-C_3N_4 nanorod.

In summary, we have developed a distinct method for the growth of single crystal β-C_3N_4 nanorods through mechanochemical reaction and subsequent thermal annealing under a streaming flow of NH_3 gas. This method is easily controllable, convenient, well-repeatable, mild, low-cost, effective, and has a large yield, and thus could be applied to the fabrication of nanorods or nanowires of related materials. Unlike previously reported results on carbon nitrides, the present result should not suffer from the obscuring signals from the substrate and contaminants and can provide direct and precise information about carbon nitride compounds.

Experimental

20 g of graphite powder with a high purity of 99.99 % was loaded into a planetary ball miller cell with several stainless steel balls. The graphite powder was first milled to a nanosized amorphous state operated under an argon atmosphere at 620 rpm (revolutions per minute) for about 50 h, and then the cell was purged with the NH_3 reaction gas and a starting pressure of 300 kPa was established prior to and during milling, after that the previously milled nanosized graphite powders were continually milled for about 70 h at 620 rpm under NH_3 atmosphere. The iron-related contaminants in the milled powder products introduced during high-energy ball milling were rigorously removed by HCl acid, followed by extensive washing by distilled water. Thermal annealing experiments for the ball milled powders were performed in a vacuum furnace at different temperature ranging from 300 °C to 450 °C under a flow of NH_3 gas. The overall chemical composition and phase structure of the synthesized carbon nitride compound nanorods were examined by means of XPS, XRD with Cu Kα radiation, and FTIR. The microstructure of the carbon nitride nanorods was analyzed in a H-800 transmission electron microscope operated at 120 kV and a JEOL JEM-3000F high-resolution field emission transmission electron microscope operated at 300 kV; parallel EELS attached to the HRTEM was used to determine the chemical composition of the carbon nitride nanorods. For FTIR measurements, the FTIR spectra were collected on a Nicolet 170 sx FTIR spectrometer with a resolution of 4 cm^{-1}.

Received: April 24, 2003
Final version: July 11, 2003
Published online: September 16, 2003

[1] S. Iijima, *Nature* **1991**, *354*, 56.
[2] E. J. M. Hamilton, S. E. Dolan, C. M. Mann, H. O. Colojin, C. A. McDonald, S. G. Shore, *Science* **1993**, *260*, 659.
[3] N. G. Chopra, R. J. Luken, K. Cherrey, V. H. Crespi, M. L. Mcohen, S. G. Louie, A. Zettl, *Science* **1995**, *269*, 966.
[4] R. Tenne, L. Margulis, M. Genut, G. Hodes, *Nature* **1992**, *360*, 444.
[5] Y. Feldman, E. Wasserman, D. J. Srolovitz, R. Tenne, *Science* **1995**, *267*, 222.
[6] Y. Li, Y. Bando, D. Golberg, *Adv. Mater.* **2003**, *15*, 581.
[7] T. Kasuga, M. Hiramatsu, A. Hoson, T. Sekino, K. Niihara, *Langmuir* **1998**, *14*, 3160.
[8] A. Y. Liu, M. L. Cohen, *Science* **1989**, *245*, 841.
[9] C. Niu, Y. Z. Lu, C. M. Lieber, *Science* **1993**, *261*, 334.
[10] D. Li, X. Chun, S. C. Cheng, X. Lin, V. P. Dravid, Y. W. Chung, *Appl. Phys. Lett.* **1996**, *68*, 1211.
[11] D. M. Teter, R. J. Hemley, *Science* **1996**, *271*, 53.
[12] M. L. Wu, M. U. Guruz, V. P. Dravid, Y. W. Chung, *Appl. Phys. Lett.* **2001**, *76*, 2692.
[13] A. J. Stevens, T. Koga, C. B. Agee, M. J. Aziz, C. M. Lieber, *J. Am. Chem. Soc.* **1996**, *118*, 10 900.
[14] H. Sjostrom, M. Stafstran, J. E. Sundgren, *Phys. Rev. Lett.* **1995**, *75*, 1336.
[15] A. Bousetta, M. Lu, A. Bensaoula, A. Schultz, *Appl. Phys. Lett.* **1994**, *65*, 696.
[16] M. Terrones, R. Kamalakaran, T. Seeger, M. Ruhle, *Chem. Commun.* **2000**, 2335.
[17] J. Wang, D. R. Miller, E. G. Gillan, *Chem. Commun.* **2002**, 2258.
[18] M. Terrones, Y.-Q. Zhu, J. P. Hare, C. L. Reeves, A. K. Cheetham, M. Rühle, H. W. Kroto, D. R. M. Walton. *Adv. Mater.* **1999**, *11*, 655.
[19] L. Hultoman, *Phys. Rev. Lett.* **2001**, *87*, 225 503.
[20] E. G. Wang, *Adv. Mater.* **1999**, *11*, 129.
[21] A. Calka, D. Wexler, *Nature* **2002**, *419*, 147.
[22] J. Wang, D. W. Wang, J. M. Xu, W. B. Ng, *Adv. Mater.* **1999**, *11*, 210.
[23] Y. Chen, J. F. Gerald, L. T. Chadderton, L. Chaffron, *Appl. Phys. Lett.* **1999**, *74*, 2782.
[24] X. H. Chen, H. S. Yang, G. T. Wu, M. Wang, F. M. Deng, X. B. Zhang, J. C. Peng, W. Z. Li, *J. Cryst. Growth* **2000**, *218*, 57.
[25] S. E. Matsumoto, Q. Xie, F. Izumi, *Diamond Relat. Mater.* **1999**, *8*, 1175.
[26] L. Guo, Y. L. Ji, H. Xu, *J. Am. Chem. Soc.* **2002**, *124*, 14 864.
[27] J. Q. Hu, Q. Li, N. B. Wong, C. S. Lee, S. T. Lee, *Chem. Mater.* **2002**, *14*, 1216.
[28] R. Soto, P. Gonzalez, F. Lusquinos, J. Pou, B. Leon, M. Perez-Amor, *Carbon* **1998**, *5–6*, 781.
[29] Y. G. Li, A. T. S. Wee, C. H. A. Huan, W. S. Li, J. S. Pan, *Surf. Interface Anal.* **1999**, *28*, 221.
[30] P. G. McCormick, T. J. Tsuzuki, S. Robinson, J. Ding, *Adv. Mater.* **2001**, *13*, 1008.
[31] J. Hu, H. Qin, Z. Sui, H. Lu, *Mater. Lett.* **2002**, *53*, 421.
[32] K. Lu, *Adv. Mater.* **1999**, *11*, 1127.

Colloidal PbS Nanocrystals with Size-Tunable Near-Infrared Emission: Observation of Post-Synthesis Self-Narrowing of the Particle Size Distribution**

By *Margaret A. Hines* and *Gregory D. Scholes**

Over the past decade tremendous efforts have been made optimizing the synthesis of semiconductor nanocrystal colloids. These "quantum dot" materials, exhibiting three-dimensional (3D) quantum confinement, are highly desired for their size-tunable optical properties. Synthetic routes utilizing organometallic precursors enable production of nanocrystalline particles with nearly monodisperse size dispersions.[1] The resulting narrow emission bandwidths and luminescence efficiencies that are achieved through these controlled syntheses[2–5] are required for applications such as optoelectronic devices[6–10] and biological fluorescence labeling.[11–13] In the

[*] Prof. G. D. Scholes, Dr. M. A. Hines
Department of Chemistry, University of Toronto
80 St. George Street, Toronto, Ontario, M5S 3H6 (Canada)
Email: gscholes@chem.utoronto.ca

[**] The Natural Science and Engineering Research Council of Canada is gratefully acknowledged for financial support. The authors wish to thank Dr. Aleksandra Perovic and Prof. Doug Perovic for the HRTEM imaging, Dr. Douglas Holmyard for the TEM imaging, Karolina Fritz for work on the aging experiments, Tihana Mirkovic for work on fluorescence measurements, Ken Lopata and Gary Iliev for their work in the characterization of the materials, and Prof. Edward H. Sargent for generous provision of his facilities.

  DOI: 10.1002/adma.200305395

present work, we report a new synthetic route for the preparation of high-quality, highly luminescent PbS nanocrystals that have bandgaps tunable throughout the near-infrared (NIR). We report studies of variations of the synthesis, including observations of shape control. Most notably, we report our observations of a fascinating focusing of the particle size distribution that occurs spontaneously over a period of hours after the product is isolated from the reaction mixture and redispersed in an organic solvent.

The explosive growth of the telecommunications industry has fueled the pursuit of luminescent quantum dots (QDs) that emit at key NIR wavelengths of 1.3 and 1.55 μm. The vast majority of colloidal QD research has focused on II–VI and III–V materials and includes substantial efforts in the development and exploration of InAs nanocrystalline materials,[14,15] although the synthesis of highly luminescent HgTe QDs has also been reported.[16] Semiconductors of group IV–VI materials, notably PbS with a bulk bandgap of 0.41 eV, offer excellent size tunability across the NIR region and can be produced with inexpensive and relatively safe synthetic precursors. We report here the synthesis of luminescent size-tunable PbS colloidal QDs.

Lead chalcogenide QDs are highly desirable as well for the strong-confinement limit offered by these small-bandgap materials. Given that most II–VI and III–V semiconductor materials have large hole masses, strong quantum confinement can be difficult to achieve. For example, as discussed by Wise,[17] InSb has an exciton Bohr radius of 54 nm but the Bohr radius of the hole is only 2 nm, thus preventing strong confinement of the hole. In comparison, the electron and hole Bohr radii of the lead chalcogenides are an order of magnitude larger and imply large confinement energies.[17] In the limit of strong confinement the third-order nonlinear optical response of PbS nanocrystals is expected to be huge, 30 times that of GaAs and 1000 times that of CdSe materials, thus rendering PbS highly desirable for photonic and optical switching device applications.

The pursuit of synthetic routes for the production of lead chalcogenide QDs is not a recent endeavor. These methods include solution phase,[18,19] gas phase,[20] and solid-state[21] syntheses, as well as polymer films,[22] and glass host fabrication.[23–25] The limitation of solution phase and gas phase syntheses is the inability to achieve tunable particle sizes. Conversely, the preparation of PbS and PbSe QDs in glass matrices has been extremely successful. These size tunable materials are narrowly dispersed, as evidenced by the well-resolved features in the absorption spectra. A major drawback shared by all of the aforementioned methods is the inability to isolate the materials readily, thus preventing incorporation into alternative media for post-synthetic applications such as device fabrication. This limitation is alleviated when working with colloidal QDs prepared by a solution phase synthesis utilizing organometallic precursors, such as that developed for the production of II–VI materials.[2]

PbS nanocrystals were synthesized by a method derived from those for cadmium chalcogenides[2,26,27] and lead selenide[28] using lead oleate and bis(trimethylsilyl)sulfide (TMS, see Experimental section for details). The absorption spectra for a range of samples are displayed in Figure 1a, demonstrating tuning from 800–1800 nm of a well-resolved lowest-energy exciton transition. The width of this band (full width at half maximum, FWHM ~ 100 meV for the peak in Fig. 1b) reflects the narrow size dispersions (10–15 %) achieved without any post-synthesis size-selective precipitation. Figure 1b shows the room-temperature absorption and photoluminescence spectra for a sample 6.5 nm in diameter. The shape of the intense photoluminescence peak indicates the emission is primarily band-edge, devoid of significant trapped-state emission. Fluorescence quantum yields for these samples were determined to be of the order ~ 20 % relative to the NIR standard dye IR125 in dimethyl sulfoxide (DMSO). We note that the measured quantum yields were found to be excitation wavelength dependent, which we find to be related to the particle size distribution.

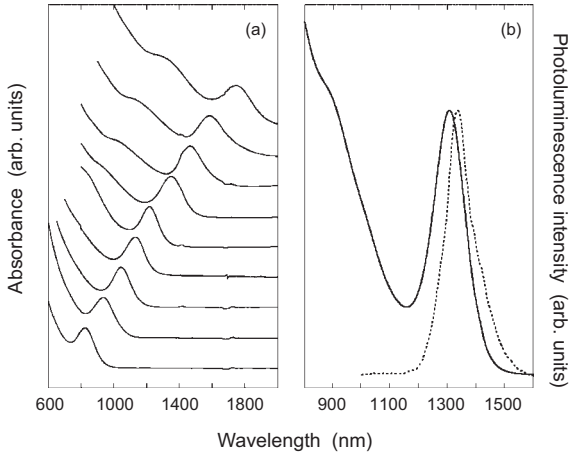

Fig. 1. Room-temperature optical characterization of toluene solutions of PbS nanocrystals. a) Absorption spectra spanning the range of tunable sizes. b) Band-edge absorption and photoluminescence peaks for a sample ~ 6.5 nm in diameter.

High-resolution transmission electron microscopy (HRTEM) images (see Fig. 2) suggest that the nanocrystals are highly crystalline and free from stacking faults and lattice defects. Energy dispersive X-ray fluorescence performed with the microscope

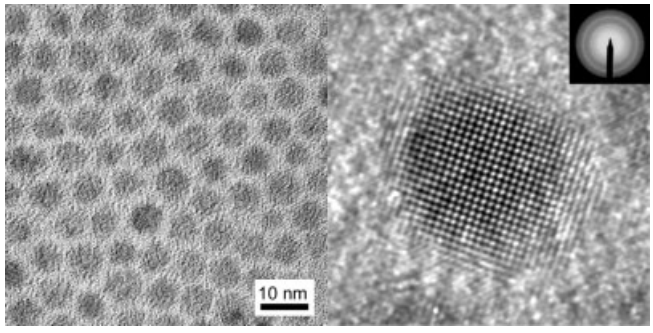

Fig. 2. HRTEM images of colloidal PbS nanocrystals with an exciton absorption at 1440 nm. The SAED spacings, inset on the single particle close-up on the right, correspond to bulk lattice parameters.

ADVANCED MATERIALS

in scanning transmission electron microscopy (STEM) mode confirmed the presence of Pb and S in the nanocrystal samples. The combined results from inductively coupled plasma/atomic emission spectroscopy (ICP/AES) and combustion elemental analysis support the expected stoichiometric ratio of 1:1 for Pb/S. Additionally, HRTEM and powder X-ray diffraction (XRD) confirmed the cubic rock salt crystal structure of the particles. The selected area diffraction (SAED) pattern, inset in Figure 2, and the imaged lattice spacings (0.59 nm oriented along the [001] direction) of the particle in Figure 2 are consistent with the rock salt structure of bulk PbS materials.

The lead and sulfur precursors readily react and easily form bulk-like particles. Thus the key to a successful PbS QD synthesis lies in a controlled nucleation event and subsequent particle growth. The stabilizing ligand and growth solvent are crucial in this regard because they influence the reactivity of the monomer species and hence aid in nanocrystal growth. Oleic acid (OA) serves well in this capacity. PbO readily dissolves in it to yield the lead oleate precursor, and the PbS nanocrystals are easily precipitated out of it with polar solvents. Most importantly, it facilitates controlled nanocrystal growth after injection of the reactants.

The nucleation and growth behavior of the PbS nanocrystals appears to be similar to that observed for CdS[29] with one notable exception: narrowly size-dispersed PbS can be successfully synthesized in large concentrations of OA. The data reported by Yu and Peng[29] correlates the role of OA concentration with monomer reactivity by examining the tunability of particle size within a given temporal window. It was found that the higher the OA concentration, the lower the monomer reactivity. When the concentration of OA is too large they found the CdS nanocrystals to be broadly dispersed in size, presumably due to a lack of a discrete nucleation event that results in uncontrolled growth onto fewer nuclei. The success of synthesizing PbS in high concentrations of OA might be attributed to the increased reactivity of the TMS precursor compared to the elemental sulfur used in the CdS synthesis.

A rapid nucleation event occurs upon injection of the S precursor into the Pb–oleate mixture as evidenced by an immediate brown color change in the reaction vessel. The remaining monomer readily feeds growth of these initial particles. When the concentration of OA is limited to a quantity just sufficient to provide ligand stabilization by diluting with octadecene in a ratio such as 4:2:1 of OA/Pb/S, the reactivity of the Pb monomer increases. In this case, the nucleation event results in a larger number of smaller particles. The color of the reaction mixture upon injection is then drastically shifted to the blue, and one can visibly see it change from yellow to brown in a few seconds. A significant difference between this PbS synthesis and that for CdS is related to the reactivity of the S precursor, TMS, versus elemental sulfur. All our synthetic efforts indicate that the reaction goes to completion—depleting the TMS entirely. This conclusion is drawn from the observation that a sulfur smell originating from the highly odiferous TMS is not detected in any reaction solution after injection. In fact, if additional TMS is added to the supernatant reaction wash left after precipitating out the PbS nanocrystals, the solution immediately turns brown, indicating a reaction with residual lead oleate. This is in contrast to the synthesis of CdS, in which there is a residual amount of unreacted Cd and S monomer present in the reaction mixture.[29] Without S monomer present to establish an equilibrium, the growth mechanism and kinetics of the PbS reaction must therefore be markedly different than the CdS reaction.

Heating the reaction mixture promotes particle growth, as evidenced by a systematic red shift of the absorption features of samples removed from the reaction mixture at different times during a period of growth at elevated temperatures. Additionally, heating has a dramatic effect on the degree of faceting of the nanocrystals. Particles isolated from aliquots removed shortly after injection appear to be highly angular according to TEM images. After heating at elevated temperatures of ~100 °C, the angular edges of the nanocrystal are observed to be more rounded. The nanocrystals largest in diameter obtained by prolonged heating appear spherical in shape by TEM compared to smaller ones that have not been heated. This observation indicates that early growth is kinetically driven, then, with time and temperature, thermodynamics gives rise to annealing of the nanocrystal surface and smoothing of the sharp edges.

A striking observation is that the nanocrystals undergo a size-focusing aging process after being isolated from the reaction mixture and redispersed in organic solvent. Figure 3a displays this dramatic result by tracking the absorption spectrum

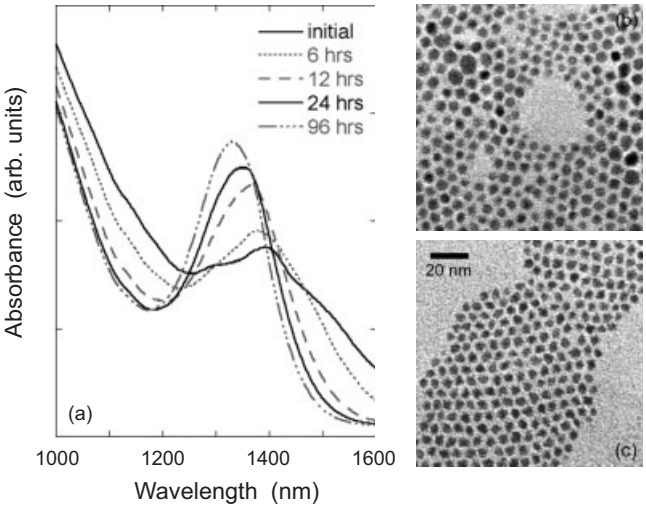

Fig. 3. a) Absorption spectra of a single toluene solution of PbS nanocrystals measured at time intervals spanning up to 96 h. The spectral evolution indicates a post-synthesis self-focusing of the size dispersion. b,c) TEM images of the nanocrystal solution taken initially (b) and at 24 h (c).

of a sample of nanocrystals over a time frame of 96 h. A sample of nanocrystals was removed after injection when the reaction cooled to 100 °C. They were purified by twice precipitating with methanol, then dispersing in toluene. The initial absorption spectrum clearly indicates that the size dispersion

of the nanocrystal sample is broad based on a poorly defined lowest-energy exciton peak. With time this spectral feature blue-shifts and sharpens, suggesting a narrowing of the size dispersion and a decrease in average particle size, most dramatically within the first 12 h. The absorption spectra presented in Figure 3 were collected with a single nanocrystal solution sample sealed in a cuvette and stored in the dark between measurements. Similar evolution of the photoluminescence is observed. Nanocrystals from the initial solution and from the solution aged for 24 h were imaged using TEM. A noticeable narrowing of the size dispersion over time is observed (see Figs. 3b,c).

Focusing of the size dispersion is not uncommon during the reaction, occurring in a regime when a suitable concentration of monomer is available to feed nanocrystal growth.[30] Eventually the monomer is consumed and the smaller particles begin to dissolve, feeding growth of the bigger nanocrystals. This Ostwald ripening results in defocusing of the size distribution. In the case of PbS nanocrystals, the self-focusing of particle size after the reaction resembles results reported for digestive ripening of gold nanoparticles by Klabunde, Sorensen, and co-workers.[31] They have extensively studied how the addition of surface active ligands can convert a toluene solution of highly polydisperse colloids into a nearly monodisperse sample with heating to the solvent boiling point. Digestive ripening occurs by larger particles breaking apart and smaller particles increasing in size until a uniform size distribution, that tends to be thermodynamically stable for the system, is achieved. For these Au nanoparticles,[31b] particle growth could occur by means of size evolution through heat-induced ligand removal and subsequent particle coalescence to form larger particles in an Ostwald ripening fashion. The shrinking of larger particles could be the result of heat-induced ligand etching. Working in conjunction, the two mechanisms would yield a smaller-sized, narrowly dispersed sample of particles. Although the results for the ripening of Au nanoparticles appear remarkably similar to those observed for PbS there are some significant differences between the processes. Additional ligand has not been added to the purified PbS nanocrystal solution. Heat is not necessary to induce the observed changes. As well, the ripened PbS particles are highly faceted, whereas the Au colloids are spherical.

Recently Landes et al.[32] have reported remarkable changes in the absorption spectrum induced by adding a large concentration of butylamine to a suspension of very small CdSe nanoparticles. They observe a blue shift and narrowing of the first absorption band of the CdSe nanocrystals after addition of butylamine. A key difference between that observation and the aging of PbS that we observe is that Landes et al. note the presence of an isobestic point in the absorption spectrum, suggesting that there are two distinct absorption features—before and after addition of butylamine. In the case of PbS, the absorption spectrum changes completely.

Further observations that indicate kinetics dominate the reaction and dictate the particles initially synthesized are the shapes of the PbS nanocrystals imaged by TEM. By modifying reaction parameters the PbS particles are seen to vary widely from bent rod-like particles to star-like polyhedrons. The variety of particle shapes observed is displayed in Figure 4. Particles removed from the reaction shortly after injection appear strongly angular and faceted (Fig. 4a). This indicates particle growth occurs along preferred crystal directions. Prolonged heating tends to smooth the particle shape, as observed by the decreased number of sharp edges on the particles in Figure 4b. Furthermore, only the larger particles that were obtained from temperature-stabilized growth appear to be symmetric in shape, with aspect ratios close to unity. Typically this was observed for particles having a lowest exciton absorption peak at ≥1400 nm. These observations suggest that particle shape engineering is feasible and will be achieved through controlling the kinetics.

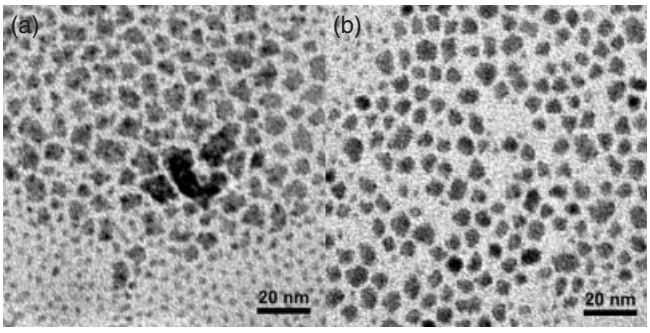

Fig. 4. TEM images of PbS nanocrystals displaying a wide variety of shapes. a) Sample removed from reaction just after injection; b) sample from same reaction removed after heating at 100 °C for 1 h.

Shape control of PbS particles, nanocrystalline but not in the size regime of quantum confinement, has been demonstrated in recent work reported by Cheon and co-workers.[33] It provides some insight into the factors underlying the ripening observed with the PbS nanocrystals. By varying the injection temperature, the shape of the resulting particles evolves from rods to multi-pods to cubes. By varying the ratio of dodecanethiol ligand to the Pb/S single source precursor, the shape can be tuned from nearly spherically shaped tetradecahedrons to almost cubic. Cheon and co-workers suggest that the dodecanethiol ligand blocks growth of the {111} faces and enhances growth on the {100} faces. On the other hand, dodecylamine, a weakly binding ligand for Pb metal atoms, promotes growth on the {111} faces, and the resulting particles are cubes.

The shapes of our PbS nanocrystals after ripening are asymmetric and distinctly polyhedral as seen in Figure 3c. The increase in faceting with aging, comparing Figures 3b,c, suggests that one crystal face is energetically favored. Based on the previous discussion of PbS materials, together with the fact that the oleate ligands are considered weakly binding, most likely it is the {111}, but further HRTEM work is underway to correlate the shape and crystal faces of the PbS particles. Any subsequent reorganization of the crystal lattice or particle growth from residual monomer species would be favored on the {111} face.

ADVANCED MATERIALS

The question that still remains to be answered is what is the driving force behind the ripening process? It is only upon isolation from the reaction solution and redispersion into an organic solvent that the PbS nanocrystals undergo the dramatic ripening process. This suggests that excess OA ligand does not mediate the process, but rather, it is solvent driven. Regardless of the driving force, the key factor remains that the as-synthesized nanocrystals are not energetically favored. One possibility that could account for such instability is that the initial particles are not a single crystal domain. This could result from rapid growth of small cluster-like particles onto existing nuclei that subsequently fall off as the crystal seeks a lower energy state with the prevalence of the {111} face. Also possible is that smaller cluster-like particles coalesce during initial growth conditions in a mismatched fashion onto the {100} crystal faces of larger particles where the ligands are not as strongly bound. Investigations are underway to determine the role that nanocrystal concentration in the toluene solution plays in the extent and rate of ripening. Investigations are also underway to assess whether the initial particle size influences the tendency of the sample to undergo ripening, in which case certain sizes might be metastable and lend themselves to magic sizes.[34]

The capping ligands on the PbS nanocrystals can be exchanged for shorter alkylamines.[35] This is useful for optimizing injection of electrons and holes into the nanocrystals by decreasing the chain length of the ligands. Such a strategy was used to improve electroluminescence efficiency from PbS nanocrystal/polymer composite films.[36] The alkylamine ligands induced etching of the nanocrystal surface—drastically shrinking the particle size, with a concommitant 200 nm shift to the blue of the lowest-energy exciton peak in the absorption spectrum. The etching was uniform, thus maintaining the initial size dispersion. This etching in neat alkylamine is not surprising given the strong ligand strength of amine. Alkylamines are also highly effective for the digestive ripening of Au colloids, as was previously discussed.[31b]

In summary, we have established a synthetic route for the production of narrowly dispersed colloidal PbS nanocrystals that offer size-tunable NIR emission. The stability and processibility of these NIR emitting QDs makes them ideal materials for device applications. The use of cost-effective and non-pyrophoric precursors, as well as the success of larger scale reactions suggests the feasibility of industrial size production of PbS nanocrystals.

Experimental

The synthesis of PbS nanocrystals was performed in a single flask. The lead oleate precursor was prepared in situ by heating PbO in OA at concentrations 0.05–0.2 M under Ar at 150 °C for 1 h. Heating under either vacuum or Ar did not appear to have any noticeable effect on the outcome of the synthesis. A solution of TMS in octadecene (ODE), a non-coordinating solvent, corresponding to a molar ratio of 2:1 Pb/S was injected into the vigorously stirring lead oleate solution at 150 °C. Trioctylphosphine (TOP) has also been used as the dilution solvent for the TMS without any perceivable effect on the resulting nanocrystals. Given that TOP is basic in chemical nature and much more reactive than ODE, it could play a greater role in the nanocrystal growth than has thus far been observed. Further work needs to be conducted before concluding that ODE and TOP are functionally interchangeable in the reaction. A typical synthesis involved 0.09 g PbO dissolved in 4 mL OA, into which 42 μL TMS in 2 mL ODE was injected. The heating mantle was lowered away from direct contact to the reaction flask immediately after injection of the TMS solution. Once the temperature of the reaction mixture reached ~100 °C the heating mantle was restored to a position against the reaction flask. Either the temperature was maintained at 80–140 °C for nanocrystal growth, or the heat was turned off to allow the reaction to cool slowly to room temperature, depending upon desired rate and final particle size.

The reaction has been successfully scaled up as much as 5× and reproducibly results in nanocrystals with the lowest-energy exciton peak positioned between 1200–1400 nm. Slightly smaller initial particle sizes are achieved by injecting the TMS at lower temperatures. Drastically smaller initial particle sizes (exciton peak positioned at 800 nm) are obtained when the amount of OA acid is reduced from a molar ratio of 32:2:1 OA/Pb/S (e.g., 0.09 g PbO dissolved in 4 mL OA) to a 4:2:1 ratio by diluting with octadecene (e.g., 0.09 g PbO dissolved in 0.25 mL OA and 3.75 mL ODE).

The nanocrystals were isolated from the growth mixture by precipitation with a polar solvent, such as methanol or acetone, and subsequently redispersed into an organic solvent such as chloroform or toluene. To insure adequate removal of the reaction solvents, precipitation and redispersion was repeated. The solvated nanocrystal dispersion was centrifuged to remove any residual reaction debris.

A FEI Technai 20 instrument equipped with a Gatan camera was used for TEM imaging to provide sizing data and particle size distributions. A JEOL-2010-FEG instrument was used for HRTEM to establish the high quality of the crystalline structure of the PbS samples. All TEM samples were prepared by placing a drop of dilute PbS/toluene solution onto a thin carbon coated copper grid and gently wicking away the excess. ICP/AES and combustion analysis of the PbS was performed at Guelph Chemical Laboratories, Guelph, ON Canada.

Absorption spectra were recorded using a Cary 500 UV/Vis/NIR spectrophotometer. Fluorescence spectra were measured using a Spex Fluorolog 3–2–2 fluorometer fitted with 1200 groove/mm gratings, blazed at 500 nm, in the excitation side, and 600 groove/mm gratings, blazed at 1000 nm, together with a liquid nitrogen cooled InGaAs diode detector on the emission side of the instrument.

Received: May 15, 2003
Final version: July 24, 2003

[1] C. B. Murray, C. R. Kagan, M. G. Bawendi, *Annu. Rev. Mater. Sci.* **2000**, *30*, 545.
[2] C. B. Murray, D. J. Norris, M. G. Bawendi, *J. Am. Chem. Soc.* **1993**, *115*, 8706.
[3] M. A. Hines, P. Guyot-Sionnest, *J. Phys. Chem.* **1996**, *100*, 468.
[4] B. O. Dabbousi, J. Rodriquez-Viejo, F. V. Mikulec, J. R. Heine, H. Mattoussi, R. Ober, K. F. Jensen, M. G. Bawendi, *J. Phys. Chem. B* **1997**, *101*, 9463.
[5] Y. W. Cao, U. Banin, *J. Am. Chem. Soc.* **2000**, *122*, 9692.
[6] V. L. Colvin, M. C. Schlamp, A. P. Alivisatos, *Nature* **1994**, *370*, 354.
[7] B. O. Dabboussi, M. G. Bawendi, O. Onitsuka, M. F. Rubner, *Appl. Phys. Lett.* **1995**, *66*, 1316.
[8] M. C. Schlamp, X. G. Peng, A. P. Alivisatos, *J. Appl. Phys.* **1997**, *82*, 5837.
[9] H. Mattoussi, L. H. Radzilowski, B. O. Dabboussi, E. L. Thomas, M. G. Bawendi, M. F. Rubner, *J. Appl. Phys.* **1998**, *83*, 7965.
[10] N. Tessler, V. Medvedev, M. Kazes, S. Kan, U. Banin, *Science* **2002**, *295*, 1506.
[11] M. Bruchez, M. Moronne, P. Gin, S. Weiss, A. P. Alivisatos, *Science* **1998**, *281*, 2013.
[12] W. C. W. Chan, S. Nie, *Science* **1998**, *281*, 2016.
[13] G. P. Mitchell, C. A. Mirkin, R. L. Letsinger, *J. Am. Chem. Soc.* **1999**, *121*, 8122.
[14] A. A. Guzelian, U. Banin, A. V. Kadavanich, X. Peng, A. P. Alivisatos, *Appl. Phys. Lett.* **1996**, *69*, 1462.
[15] X. Peng, J. Wickham, A. P. Alivisatos, *J. Am. Chem. Soc.* **1998**, *120*, 5343.
[16] A. L. Rogach, S. V. Kershaw, M. Burt, M. Harrison, A. Kornowski, A. Eychmüller, H. Weller, *Adv. Mater.* **1999**, *11*, 552.
[17] F. W. Wise, *Acc. Chem. Res.* **2000**, *33*, 773.
[18] M. T. Nenadovice, M. I. Comor, V. Vasic, O. I. Micic, *J. Phys. Chem.* **1990**, *94*, 6390.
[19] T. Trindade, P. O. O'Brien, X. Zhang, M. J. Motevalli, *Mater. Chem.* **1997**, *7*, 1011.
[20] C. Kaito, Y. Saito, K. Fujita, *Jpn. J. Appl. Phys.* **1987**, *26*, 1973.

[21] W. Wang, Y. Liu, Y. Zhan, C. Zheng, G. Wang, *Mater. Res. Bull.* **2001**, *36*, 1977.
[22] S. H. Wang, S. H. Yang, *Langmuir* **2000**, *16*, 389.
[23] N. F. Borrelli, D. W. Smith, *J. Non-Cryst. Solids* **1994**, *180*, 25.
[24] A. Lipovskii, E. Kolobkova, V. Petrikov, I. Kang, A. Olkhovets, T. Krauss, M. Thomas, J. Silcox, F. Wise, Q. Shen, S. Kycia, *Appl. Phys. Lett.* **1997**, *71*, 3406.
[25] A. A. Lipovskii, E. V. Kolobkova, A. Olkhovets, V. D. Petrikov, F. Wise, *Phys. E* **2000**, *5*, 157.
[26] Z. A. Peng, X. Peng, *J. Am. Chem. Soc.* **2001**, *123*, 183.
[27] L. Qu, Z. A. Peng, X. Peng, *Nano Lett.* **2001**, *1*, 333.
[28] C. B. Murray, S. Sun, W. Gaschler, H. Doyle, T. A. Betley, C. R. Kagan, *IBM J. Res. Dev.* **2001**, *45*, 47.
[29] W. W. Yu, X. Peng, *Angew. Chem. Int. Ed.* **2002**, *41*, 2368.
[30] X. G. Peng, J. Wickham, A. P. Alivisatos, *J. Am. Chem. Soc.* **1998**, *120*, 5343.
[31] a) X. M. Lin, C. M. Sorensen, K. J. Klabunde, *J. Nanopart. Res.* **2000**, *2*, 157. b) B. L. V. Prasad, S. I. Stoeva, C. M. Sorensen, K. J. Klabunde, *Chem. Mater.* **2003**, *15*, 935.
[32] C. Landes, M. Braun, C. Burda, M. A. El-Sayed, *Nano Lett.* **2001**, *1*, 667.
[33] a) S.-M. Lee, Y.-W. Jun, S.-N. Cho, J. Cheon, *J. Am. Chem. Soc.* **2002**, *124*, 11 244. b) S.-M. Lee, S.-N. Cho, J. Cheon, *Adv. Mater.* **2003**, *15*, 441.
[34] A. W. Castleman, K. H. Bowen, *J. Phys. Chem.* **1996**, *100*, 12 911.
[35] The nanocrystal powder is dispersed in a suitable amount of amine, such as octylamine, and stirred for several days. The nanocrystals are precipitated with dimethylformamide (DMF) and the procedure repeated. The final resulting nanocrystal powder is dispersible in non-polar solvents.
[36] L. Bakoueva, S. Mushikin, M. A. Hines, T.-W. F. Chang, M. Tzolov, G. D. Scholes, E. H. Sargent, *Appl. Phys. Lett.* **2003**, *82*, 2895.

Nanotubes Prepared by Layer-by-Layer Coating of Porous Membrane Templates**

By *Zhijian Liang*, *Andrei S. Susha*, *Aimin Yu*, and *Frank Caruso**

Since the discovery of carbon nanotubes,[1] one-dimensional nanostructured materials, such as nanowires and nanotubes (NTs), have attracted intense scientific interest because of their potential application in optical, electronic, and magnetic devices.[2,3] A common route to prepare nanowires and NTs[4–8] of different composition has been via membrane template-directed syntheses. Membranes used for templating, for example, alumina and polycarbonate (PC), contain vertically oriented pore arrays. By filling the cylindrical pores of the membranes with various materials, nanowires and NTs of metals,[5–7,9] inorganic oxides,[10,11] semiconductors,[12–15] polymers,[8,16,17] and carbon[18–20] have been prepared. Methods used to synthesize NTs in the pores of template membranes include electroless metal deposition,[9] sol–gel chemistry,[10,11] electrochemical deposition,[5–7] chemical vapor deposition,[21] and melting or dissolving polymer into the pores.[8,16,17] The size and the structural properties of the materials prepared by membrane templating are determined by the morphology of the templates employed. Highly-ordered nanowire and NT arrays can be obtained by using alumina membranes that contain highly-ordered pores.[7]

The layer-by-layer (LbL) method,[22,23] recognized as a premier technique for the preparation of multilayer films, largely due to its low cost, simplicity, and versatility, also has potential for the preparation of designed nanotubes. This technique, which primarily exploits the electrostatic attraction between oppositely charged species deposited from solution, has been widely used to prepare multilayer films, both on planar supports[22–25] and, recently, on colloid particles.[26–31] The LbL technique permits the coating of substrates of various shapes and sizes with uniform layers of varying composition (polymers, biological macromolecules, dyes, and nanoparticles) and controllable thickness (nanometer resolution). However, previous studies have employed mostly nonporous substrates for coating, with relatively few reports focusing on the use of highly porous supports.[32–38] For example, polyelectrolyte (PE)/semiconductor nanoparticle (CdTe NPs) multilayers have been deposited onto macroporous (inverse opal) titania structures by the LbL method to yield heterogeneous inverse opaline materials.[32] In other work, Bruening and co-workers prepared PE multilayers on top of alumina membranes with pore sizes of ~20 nm by the LbL method for ion transport investigations.[33] These studies showed that the underlying pores of the membranes were not "clogged" with PE, suggesting small amounts of PE were deposited in the pores of the alumina membranes, with a thin film forming on top of the membrane after the deposition of five PE bilayers.[33] Previous LbL studies have not emphasized PE coating of the pores of membrane templates, and moreover, they have not dealt with the possible preparation of nanotubes from LbL-coated porous templates.

In this work, we report the LbL templating of porous membranes to produce PE and PE/nanoparticle (NP) hybrid NTs. PC membranes containing cylindrical pores of diameter 400 nm and a pore depth of 10 μm were used. The procedure for preparation of the NTs involves three main steps (Fig. 1): 1) LbL deposition of oppositely charged PEs (or PEs and nanoparticles) onto the membranes, including the inner surfaces (i.e., pores); 2) mechanical removal of the layers deposited on the top and bottom surfaces of the membranes; and 3) membrane dissolution, achieved by exposure to a suitable solvent (e.g., dichloromethane). The main advantages of this approach for forming NTs are: i) it offers a facile route to NT production, as it is based on electrostatic self-assembly principles, thereby being applicable to a wide range of materials and hence allowing the preparation of NTs of diverse composition; ii) it provides control of the length and diameter of the NTs, determined by the template used; and iii) it affords

[*] Prof. F. Caruso, Dr. Z. Liang
Department of Chemical and Biomolecular Engineering
The University of Melbourne
Victoria 3010 (Australia)
E-mail: fcaruso@unimelb.edu.au
Dr. A. S. Susha, Dr. A. Yu
Max Planck Institute of Colloids and Interfaces
D-14424 Potsdam (Germany)

[**] This work was supported by the DFG and the Australian Research Council (Discovery Project and Federation Fellowship Schemes). We thank P. Schuetz and F. Meiser for assistance with electron microscopy measurements, I. Radtchenko for confocal microscopy, and N. Gaponik for providing the CdTe nanoparticle sample. H. Möhwald is thanked for supporting this work within the MPI interface department, and the Particulate Fluid Processing Centre (Melbourne University) for infrastructure support.

 DOI: 10.1002/adma.200305580